

Self-heating in a GaN based heterostructure field effect transistor: Ultraviolet and visible Raman measurements and simulations

I. Ahmad,^{a)} V. Kasisomayajula, D. Y. Song, L. Tian, J. M. Berg, and M. Holtz^{b)}
Texas Tech University, Lubbock, Texas 79409

(Received 10 July 2006; accepted 13 September 2006; published online 8 December 2006)

We report direct self-heating measurements for AlGaIn/GaN heterostructure field effect transistor grown on SiC. Measurements are carried out using micro-Raman scattering excited by above band gap ultraviolet and below band gap visible laser light. Ultraviolet excitation probes the GaN near the AlGaIn/GaN interface region of the device where the two-dimensional electron gas carries the source-drain current. The visible excitation probes the entire $\sim 1 \mu\text{m}$ thick GaN layer and the SiC substrate near the interface with GaN. These results thus provide a measure of the average temperature throughout the GaN and of the substrate. Results are backed by combined electrical and thermal simulations. We find that the immediate hot spot region of the device, at the edge of the gate electrode, rises by up to $\sim 240^\circ\text{C}$ over ambient under the most aggressive drive conditions examined. © 2006 American Institute of Physics. [DOI: 10.1063/1.2395681]

I. INTRODUCTION

Intense research in devices based on wide band gap AlGaIn semiconductors stems from favorable properties for producing high power electronic devices operating at high temperatures and under hostile environments.¹ Epitaxial AlGaIn has been used to make heterostructure field effect transistors (HFETs) for high power and high temperature applications.² AlGaIn/GaN HFETs have been pseudomorphically grown on sapphire and SiC substrates, and on bulk GaN.^{3,4} Comparative studies of HFETs grown on different substrates favor devices grown on SiC.⁴ This is attributable to the higher thermal conductivity of SiC, ten and three times greater than those of sapphire⁵ and GaN,⁶ respectively, allowing better heat dissipation from the active region.

In this paper we examine Joule heating in an AlGaIn/GaN HFET composed of a thick ($\sim 1 \mu\text{m}$) GaN layer capped with a thin (32 nm) AlGaIn layer. The AlGaIn/GaN band offset, piezoelectric field, and spontaneous polarization field occurring in the structure create a quasi two-dimensional electron gas (quasi-2DEG) at the interface with very high free-electron concentration located in the GaN at the interface with the AlGaIn. The source-drain current is confined to flow in this 2DEG.⁷ Because the current density can be commensurately high, collisional energy loss from electrons to the crystal leads to *self-heating*.

Electron energy loss can be decomposed into ionized defect-related scattering and electron-phonon interaction.⁸ The ionized defect scattering is generally important at low temperatures and its importance also diminishes with increased free-carrier concentrations due to screening. The Fröhlich interaction is the primary electron-phonon mechanism responsible for electron energy loss in polar semiconductors, such as GaN. In either the three- or two-dimensional

form, the Fröhlich interaction is strongest for zone-center longitudinal optic phonons.⁹ In the 2DEG device structure studied here, the channel current is predominantly transverse to the (0001) crystal axis and so electron-phonon energy transfer is expected to emit primarily $\mathbf{k}=0$ phonons with $E_1(\text{LO})$ symmetry.

The eventual performance of high power high-frequency AlGaIn/GaN HFETs is limited by self-heating. Thermal management approaches include the employment of substrates with superior thermal conductivity (e.g., SiC), flip-chip bonding, and peak electric field reduction. Various designs have been used to tailor the electric field for the purpose of reducing the impact of Joule heating.¹⁰ However, reliability remains a major concern and transport properties degrade with increasing temperature. To optimize the device design for reliability and performance, direct measurement of temperature in the active region is essential. Temperature measurements by infrared techniques are limited by lateral resolution on the order of tens of microns,¹¹ whereas high power HFETs have sizes on the order of microns.

Micro-Raman spectroscopy has been used to measure the temperature of AlGaIn/GaN HFETs.¹²⁻¹⁴ In this approach the temperature dependence of the GaN E_2^2 phonon energy is used as a measure of the lattice temperature. In all but one study to date,¹³ visible light is used as Raman excitation source. Since GaN is transparent to visible light these measurements correspond to an *average* temperature throughout the depth and do not directly address the hottest current channel region of the 2DEG.

The objective of this work is to develop UV micro-Raman spectroscopy^{13,15} to study the temperature distribution in an operating HFET structure. We use micro-Raman spectroscopy with near band gap excitation (363.8 nm), which has a shallow penetration depth in GaN,¹⁶ to probe the device active region. The results are directly compared with standard visible micro-Raman measurements of the average temperature in the HFET. An added bonus of the visible micro-Raman measurements is the substrate temperature

^{a)}Present address: Department of Electrical Engineering, Virginia Commonwealth University, Richmond, VA.

^{b)}Author to whom correspondence should be addressed; electronic mail: mark.holtz@ttu.edu

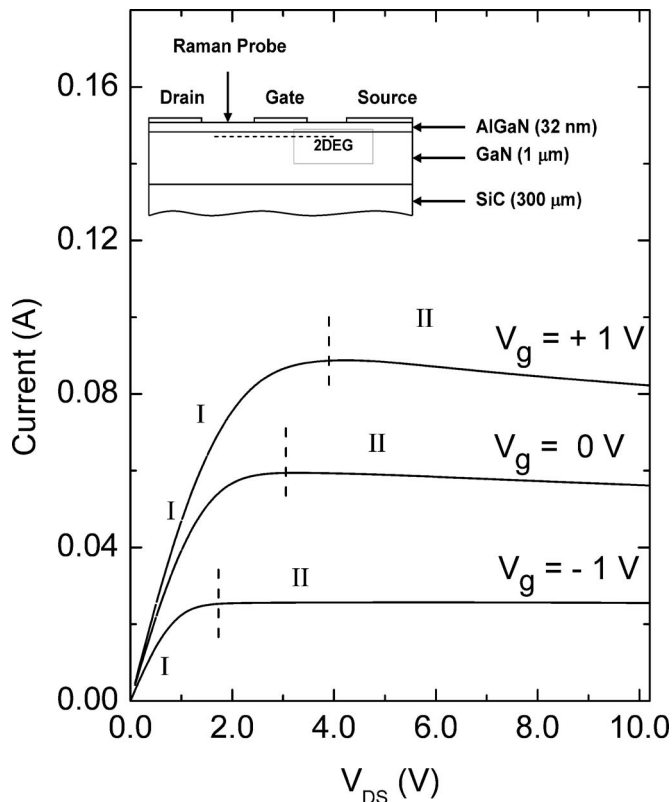


FIG. 1. I - V dependence for the AlGaIn/GaN HFET at different V_g . Inset: device layout (not to scale).

from induced shifts of SiC phonons. We thus demonstrate a temperature depth profile in the HFET structure obtained at the edge of the gate. To better describe the experimental results we also performed coupled electrical and thermal simulations using finite difference (FD) and finite element (FE) methods, respectively. Literature values of the material properties were utilized for all simulations. We obtain excellent agreement between the simulation and experimental results. We thus establish a proper and reliable way to measure and simulate self-heating in AlGaIn/GaN HFET structures under operation. The methods can be readily extended to other devices.

II. EXPERIMENTAL DETAILS

The basic device structure is depicted in the inset of Fig. 1. Details have been previously described.² A 50 nm AlN nucleation layer (not shown) was used to initiate GaN growth on a 6H-SiC substrate. The thickness of the GaN buffer layer was 1 μ m with unintentional n -type doping level of 4×10^{17} cm⁻³. Al_{0.19}Ga_{0.81}N (32 nm thick) was grown as a barrier layer. Ohmic drain (D) and source (S) (Ti/Al/Ni/Au) and Schottky gate (oxidized Ni and Au) contacts were deposited. The drain and source are separated by 5 μ m gap with 2 μ m gate at the center of the drain-source gap. The spaces (1.5 μ m) between source and gate, and gate and drain provide windows for micro-Raman studies.

Figure 1 shows the I - V characteristics. Circles are the measured I - V and curves are results of simulations described in Sec. IV. The decrease in current at higher drain-source voltage (V_{DS}) signifies strong self-heating. We divide the

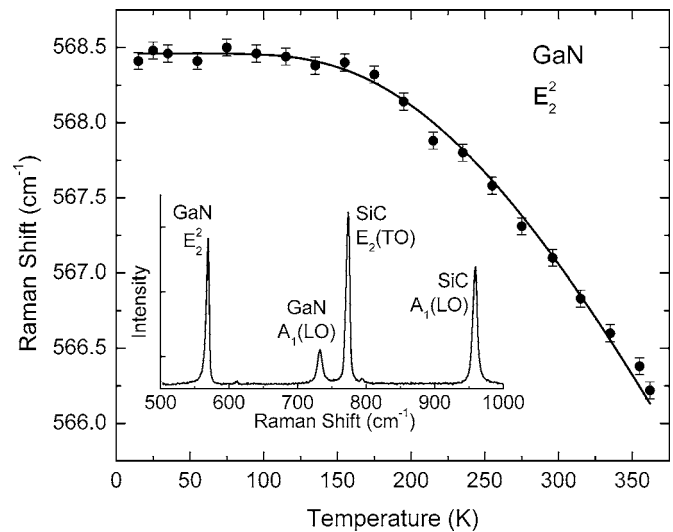


FIG. 2. Summary of E_2^2 phonon energy vs temperature used for calibration. The inset is an example Raman spectrum (488.0 nm excitation, room temperature) showing symmetry allowed E_2^2 and $A_1(LO)$ lines from the GaN layer as well as the $E_2(TO)$ and $A_1(LO)$ lines from the 6H-SiC substrate. Fit results are described in Ref. 20.

I - V characteristics into two regions demarked by vertical lines. Region I is the region after which velocity saturates and 2DEG is depleted on the drain side. Region II shows the current to diminish with increasing V_{DS} which is attributed to strong self-heating effects.

Micro-Raman measurements were used to determine the temperature of the AlGaIn/GaN HFET based on the E_2^2 phonon shift. We rely on calibrated shifts of the E_2^2 phonon to determine the temperature. We prefer these measurements to the alternative approach of determining temperature via the Stokes to anti-Stokes intensity ratio. The Stokes/anti-Stokes method may be useful for the visible measurements, where optical penetration exceeds the layer thickness. Near the absorption edge, however, differences in the absorption coefficient will strongly affect the relative intensities making temperatures difficult to extract based on these intensities.

Excitation sources for our measurements were Ar⁺ ion laser 363.8 and 488.0 nm lines. Each was focused into the device window near the gate edge. For visible Raman, the scattered radiation was analyzed by a 0.5 m spectrometer and detected using a liquid N₂ cooled charged coupled device (CCD) array. The system was calibrated with spectral lines from a Ne lamp and the argon plasma lines. An example spectrum (488.0 nm) is shown in the inset of Fig. 2. For the UV Raman work, a 0.78 m scanning monochromator was used with a photomultiplier. The spectral resolution of the system was 2.0 cm⁻¹. The measurements were performed in backscattering configuration with incident light along the (0001) crystal axis of the GaN. In this geometry the GaN E_2^2 -symmetry phonon and 6H-SiC $A_1(LO)$ and $E_2(TO)$ phonons are Raman active.

In Raman backscattering the excitation is attenuated as it travels through the material and the scatter is attenuated as it returns toward the surface. Each of these attenuation factors is exponential. The net result is that the scattering intensity coming from depth z is proportional to $\exp[-(\alpha_L + \alpha_S)z]$,

where α_L and α_S are the attenuation coefficients for laser (λ_L) and scattered (λ_S) light, respectively. The net attenuation coefficient for Raman backscatter is thus the sum of these attenuation coefficients and the optical penetration depth is $d_{\text{opt}} = 1/(\alpha_L + \alpha_S)$. For sub-band-gap excitation, as in the case of our visible excitation, $\alpha_L \approx \alpha_S$ and therefore $d_{\text{opt}} \approx 1/(2\alpha_L) \gg 1 \mu\text{m}$. However, for excitation near the band gap the attenuation coefficient changes rapidly with wavelength and d_{opt} must be determined using α_L and α_S at the excitation and emission wavelengths. This is the case for our UV micro-Raman measurements.

The attenuation coefficient for the GaN is calculated using published spectroscopic ellipsometry measurements.¹⁶ Using values of α for $\lambda_L = 363.8 \text{ nm}$ and redshifted by the E_2^2 phonon we calculate $d_{\text{opt}} \leq 100 \text{ nm}$ with UV excitation. Thus, the measured phonon shifts due to self-heating will give us a measure of the temperature near the 2DEG (363.8 nm laser) and averaged throughout the GaN layer (488.0 nm laser). Since GaN is transparent at 488.0 nm, we obtain the SiC temperature from the visible Raman measurements and within the top $< 10 \mu\text{m}$ near the GaN/SiC interface, as dictated by the microscope objective depth of focus. These measurements allow us to quantitatively and directly study the temperature distributions at these three depths of the devices and with $\sim 1 \mu\text{m}$ lateral resolution.

III. CALIBRATION OF TEMPERATURE BASED ON RAMAN MEASUREMENTS

With increasing temperature, the GaN E_2^2 phonon redshifts and broadens. The shift is used to experimentally determine the lattice temperature based on calibration curves. To obtain these curves we carried out controlled studies of the GaN E_2^2 phonon for the HFET device (unpowered) far from the device region. The sample is mounted in a cryostat and the conditions varied systematically with Raman measurements at each temperature. This approach was used to minimize the effects of substrate stress on our calibration, although it does not account for shifts induced by thermal stress due to local temperature gradients. Figure 2 shows the calibration results for the E_2^2 phonon. The phonon redshift in high-quality materials can be interpreted based on phonon decay according to¹⁷

$$\omega(T) = \omega_0 - \Delta_1(T) - \Delta_2(T), \quad (1)$$

where ω_0 is the harmonic frequency of the phonon mode, $\Delta_1(T)$ is the thermal expansion contribution to the frequency, and $\Delta_2(T)$ is the anharmonic interaction term. The thermal expansion contribution is given by

$$\Delta_1(T) = \omega_0 \gamma \int_0^T [\beta_c(T') + 2\beta_a(T')] dT', \quad (2)$$

where γ is the Grüneisen parameter and β_c (β_a) is the temperature dependent linear thermal expansion coefficient parallel (perpendicular) to the hexagonal c axis.¹⁸ The expression for Δ_1 introduces no fitting parameters. The anharmonic contribution to the phonon shift $\Delta_2(T)$ is¹⁹

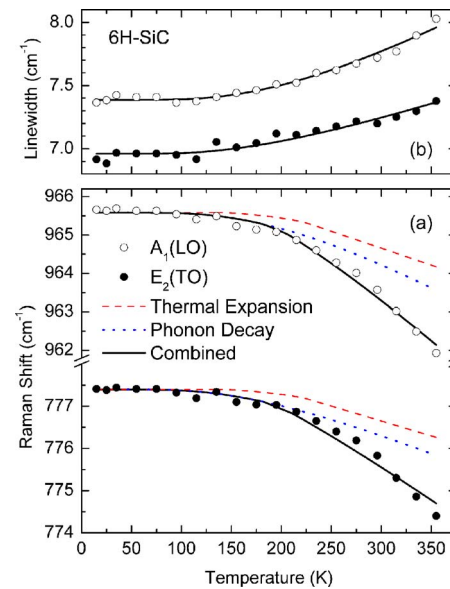


FIG. 3. (Color online) (a) SiC phonon energy vs temperature used for calibration. The solid curves are fit results using thermal expansion and phonon decay effects (individual contributions to the dependence are shown as dashed and dotted curves, respectively). (b) shows phonon linewidth vs temperature with fitted results of the phonon decay.

$$\begin{aligned} \Delta_2(T) = & A[1 + n(\omega_1, T) + n(\omega_2, T)] + B[1 + n(\omega_3, T) \\ & + n(\omega_4, T) + n(\omega_5, T) + n^2(\omega_3, T) + n^2(\omega_4, T) \\ & + n^2(\omega_5, T)], \end{aligned} \quad (3)$$

where $n(\omega, T) = [\exp(hc\omega/k_B T) - 1]^{-1}$ is the Bose function at energy $hc\omega$ (phonon energy ω is expressed in cm^{-1}). The first term in Eq. (3) corresponds to the two-phonon decay process, where ω_1 and ω_2 are frequencies of the two phonons created by the decay. The second term in Eq. (3) corresponds to the three-phonon decay process with energies ω_3 , ω_4 , and ω_5 . In both cases, the created/annihilated phonon energies must satisfy conservation of energy. For the zone-center Raman-active phonons, crystal momentum conservation requires the sum of the wave vectors of the created phonons in the decay process to be zero. Anharmonic constants A and B identify the relative probabilities of the decay processes.

Recently, Song *et al.* have carried out extensive Raman studies concerning thick layers of GaN, for which the substrate stress is negligible and the material is of high quality.²⁰ The E_2^2 phonon temperature dependence is found to be primarily influenced by the $\Delta_1(T)$ term in Eq. (1) due to the absence of two-phonon decay channels. The weaker three-phonon decay mechanism contributes a small amount to the observed shift, and consequently the dependence seen in Fig. 2 is gradual.

To determine the temperature of the substrate we use the superimposed Raman bands of the 6H-SiC substrate obtained during the visible Raman measurements of the HFET structure. Two bands are observed at 964 and 776 cm^{-1} (room temperature) identified as the $A_1(\text{LO})$ and $E_2(\text{TO})$ Raman-active phonons, respectively. A calibration procedure identical to that employed for GaN was adopted. Figure 3 shows the experimental temperature dependence of SiC phonon energies and linewidths along with the fit using Eqs.

TABLE I. Fitting parameters for 6H-SiC phonons.

Symmetry	Energy	Linewidth	Decay phonons
$A_1(\text{LO})$	$\omega_0=971.5 \text{ cm}^{-1}$ $A=5.9 \text{ cm}^{-1}$	$\Gamma_0=5.7 \text{ cm}^{-1}$ $C=1.7 \text{ cm}^{-1}$	$\omega_1=551.7 \text{ cm}^{-1}$ $\omega_2=419.8 \text{ cm}^{-1}$
$E_2(\text{TO})$	$\omega_0=780.4 \text{ cm}^{-1}$ $A=3.0 \text{ cm}^{-1}$	$\Gamma_0=6.2 \text{ cm}^{-1}$ $C=0.8 \text{ cm}^{-1}$	$\omega_1=389.6 \text{ cm}^{-1}$ $\omega_2=390.8 \text{ cm}^{-1}$

(1)–(3). Literature values of the thermal expansion coefficients²¹ have been used in Eq. (2); it has been recently found that the temperature dependence of these coefficients are important in fitting the phonon energy dependence.²⁰ The Grüneisen parameter was taken from Ref. 22. Also shown in Fig. 3(b) are the temperature dependences of the SiC phonon linewidths. The broadening is described by phonon decay (lifetime) according to

$$\Gamma(T) = \Gamma_0 + \Delta'_2(T), \quad (4)$$

where $\Delta'_2(T)$ is identical in form to $\Delta_2(T)$ with $A(B)$ replaced by $C(D)$ and the ω_i energies are the same as what we obtain from fitting Eqs. (1)–(3) to the phonon energy data. For both $A_1(\text{LO})$ and $E_2(\text{TO})$ bands the two-phonon decay mechanism is sufficient to describe the anharmonic contributions seen in both phonon shift and broadening (Table I). The zone-center $A_1(\text{LO})$ phonon decays asymmetrically to two phonons with energies of 552 and 420 cm^{-1} . In the case of the zone-center $E_2(\text{TO})$ phonon, the decay is symmetric into two phonons at 390 cm^{-1} .

The calibration dependences for both GaN and SiC are thus used in conjunction with the measured E_2^2 phonon energy to determine the temperature in the self-heating measurements. Changes in the linewidths are too small to use for estimating the temperature over the ~ 100 K range measured in our HFET experiments.

IV. COUPLED ELECTRICAL AND THERMAL SIMULATIONS

We use a commercial software package²³ to compute the electrical transport properties in the HFET structure. This program uses the finite difference method to self-consistently solve the Schrödinger and Poisson equations. In this approach, the potential function V is first obtained from the Poisson equation relying on an initial guess of the mobile charge density. The calculated potential is used in the Schrödinger equation, and the electron energy levels and eigenfunctions are then calculated. These energy levels and wave functions are subsequently used to calculate the electron density obeying Fermi statistics. The calculated electron density is inserted back into the Poisson equation to determine the potential. The procedure is repeated iteratively until convergence is achieved. Figure 4 shows the simulated conduction band and electron density distribution along the depth axis of the AlGaIn/GaN HFET and under quiescent conditions. This simulation agrees with previously published dependences² and illustrates the very high free-electron concentration at the interface between the AlGaIn and GaN

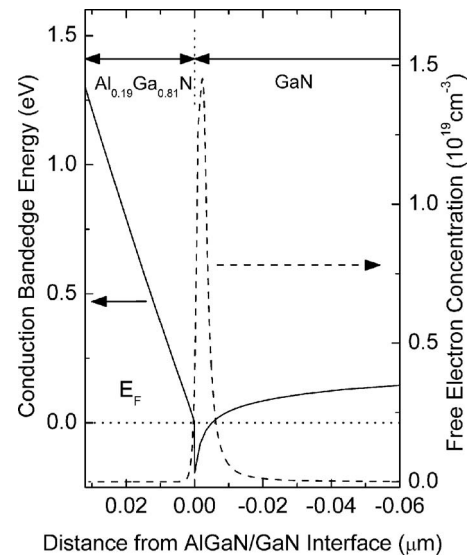


FIG. 4. Calculated conduction band edge dependence with depth. The AlGaIn/GaN interface is at the origin. Also shown is the calculated free-electron density illustrating the presence of a dense 2DEG.

present due to the band discontinuity. The peak electron concentration in this quasi-2DEG is in excess of 10^{19} cm^{-3} .

The dynamical behavior of a device is described by the drift-diffusion model. The model describes characteristics such as signal amplification, current flow, and electric field provided the device dimensions exceed the electron mean free paths. In our simulation the drift-diffusion model and Poisson equation are solved together with continuity equation in a scheme proposed by Azoff.²⁴ In this scheme the model assumes the electrostatic potential to continuously follow the vacuum levels.²⁵ The simulation results in the electrical properties of the device under different operating conditions.

The important quantities obtained are electric field, electron density, and current density throughout the HFET structure under boundary conditions specified by the drain, source, and gate voltages. We observe the characteristic high field region on the drain side when operating the device in the saturation regime. The electron density decreases dramatically in this voltage range, dropping by over two orders of magnitude at the gate edge in the 2DEG region. To obtain the power dissipated by the electron current we make use of the field (E) dependent velocity characteristics for GaN given in Ref. 8. The power delivered by the electrons to the lattice is given by

$$P_v = nev_d(E)E, \quad (5)$$

where P_v is the power density per unit volume, n is the electron density, e is the charge of the electron, and $v_d(E)$ is the field dependent drift velocity.²⁶ The position dependence has been suppressed in Eq. (5). Peak electric fields on the order of 1 MV/cm are obtained in the 2DEG region for source-drain voltage of 6 V and $V_g=0$ V, in reasonable agreement with Ref. 27. Figure 5(a) shows the simulated power density under these drive conditions. We observe higher power density on the drain side at the edge of the gate, i.e., in the pinch-off region. Power density distributions,

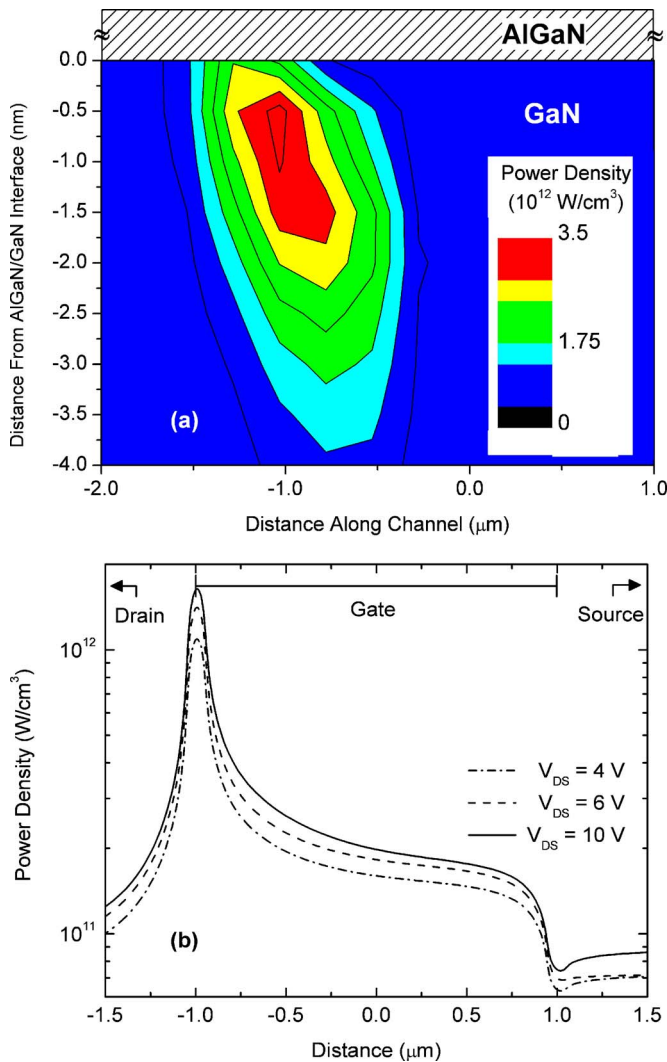


FIG. 5. (Color online) (a) Cross section of the simulated power density illustrating the presence of a power spike ($V_{DS}=+4$ V; source and gate grounded, not to scale). (b) Power density along the 2DEG for several drive conditions with $V_g=0$.

like that shown in Fig. 5(a), are simulated under gate and drain-source drive voltage conditions used in the Raman studies. The results of these simulations are averaged through the thickness of the 2DEG. Example results are shown in Fig. 5(b). In these simulations, corresponding to above-saturation conditions, power delivery takes place primarily in a narrow zone with power density one order of magnitude above the remainder of the channel region. These results are then used directly in our thermal simulations. We find that average values of the power density across the 2DEG depth adequately describe the heat input.

Thermal simulations were conducted using the finite element approach²⁸ with the power density simulation results P_v as input. In steady state the heat conduction equation is

$$\vec{\nabla} \cdot [\kappa \vec{\nabla}(\eta)] + P_v = 0, \quad (6)$$

where $\eta = T - T_0$ is the temperature difference from ambient temperature T_0 and κ is the thermal conductivity. Standard boundary conditions are applied to the HFET structure,

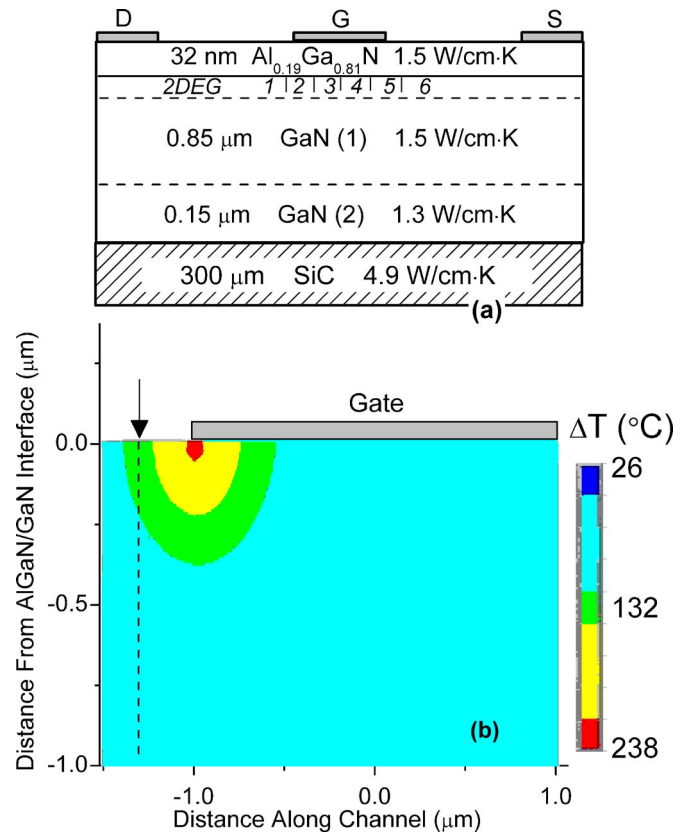


FIG. 6. (Color online) (a) Basic configuration of our thermal analysis (not to scale). (b) Example of finite element simulation illustrating the presence of the hot spot where the power spike resides. Conditions are the same as in Fig. 5.

$$\eta|_{\text{extended boundaries}} = 0 \quad \text{and} \quad \left. \frac{\partial \eta}{\partial z} \right|_{\text{top}} = 0. \quad (7)$$

Equation (6) was used in its discrete form to calculate the temperature rise (ΔT). The discrete form of the equation was then solved at each node of the finite element mesh.

The design for our thermal analysis simulation²⁸ is depicted in Fig. 6(a). Heat was input in a thin slab at the AlGaIn/GaN interface, corresponding to the 2DEG, using different heating zones (1 through 6 in the figure) in this layer. The number and lateral widths of the heat generation regions were adapted to rapid/slow variations in the power distribution from our electrical simulation; these results depend on the applied drain-source voltage. Thermal conductivities (κ) of GaN are known to depend on the dislocation density (ρ_D),⁶ which varies along the epitaxial growth direction. Recent x-ray diffraction studies of GaN grown on SiC show the dislocation density to be high in the initial growth region.²⁹ We divide the GaN layer in our simulations into two layers. In Fig. 6(a) layer 1 is the bulk of the GaN layer with $\rho_D < 10^9$ cm⁻² and $\kappa_1 = 1.5$ W/cm K.⁶ GaN layer 2 is the 150 nm thick initial growth layer with $\rho_D \sim 10^{11}$ cm⁻² and $\kappa_2 = 1.3$ W/cm K. We take into account the temperature dependence of these values according to Ref. 30. Since the thin AlGaIn plays a minor role in dissipating heat, we employ the properties of GaN. We use $\kappa_3 = 4.9$ W/cm K for SiC.⁵ Because the observed ΔT rise in the SiC is small we ignore its temperature dependence. No thermal boundary resistance

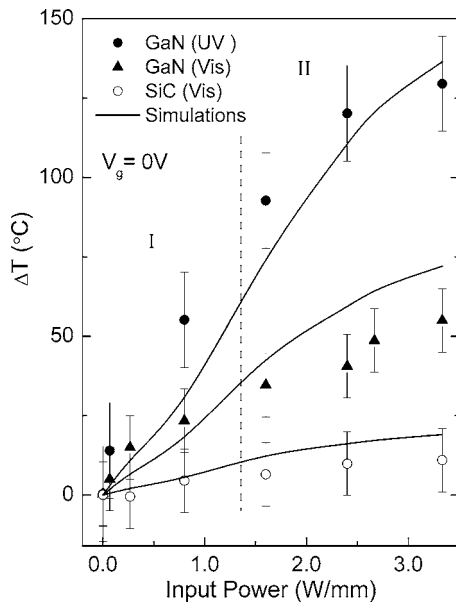


FIG. 7. Measured and simulated rises in temperature with input power taken at the gate edge on the drain side of the gate. The three data sets correspond to UV near 2DEG (filled circles), visible GaN average (filled triangles), and substrate (open circles).

at the GaN/SiC interface was necessary in our thermal analysis.³¹ Use of a realistic high defect density GaN layer (layer 2) eliminates the need for thermal boundary resistance at the GaN/SiC interface in our thermal simulations.

Figure 6 shows the temperature rise in the AlGaIn/GaN HFET structure for $V_{DS}=6$ V and $V_g=0$ V. The power dissipation spike seen on the drain side of the gate produces high local heating in this region (~ 0.5 μm from the gate edge). The simulated temperature rise (ΔT) is obtained along the dashed curves in Fig. 6(b), approximating the position where the micro-Raman probe is positioned. A rapid decrease in temperature from 75 to 50 $^{\circ}\text{C}$ is observed in the initial 1.0 μm of the device. This rapid fall in temperature is expected due to the high thermal conductivity of SiC (approximately two times higher than the GaN thermal conductivity). To approximate the Raman probe measurements volume averages of the temperature were taken in the top 60 nm, throughout the entire 1.0 μm GaN layer, and in the topmost 10 μm of the SiC substrate.

V. COMPARING SIMULATION AND MEASURED RESULTS

Figure 7 shows the experimental results of temperature rise in the GaN based HFET operating under different drive conditions and zero gate voltage. We observe that the temperature rise measured by UV micro-Raman is consistently twice that measured using visible excitation. We also observe that the temperature rise of the substrate is very small compared to the GaN temperature. These observations are qualitatively consistent with the self-heating taking place in the 2DEG.

The curves in Fig. 7 are the results of the coupled electrical and thermal simulations for different V_{DS} and zero gate voltage. The simulations for +1 and -1 V gate voltage were also performed¹³ to investigate the effect of gate voltage on

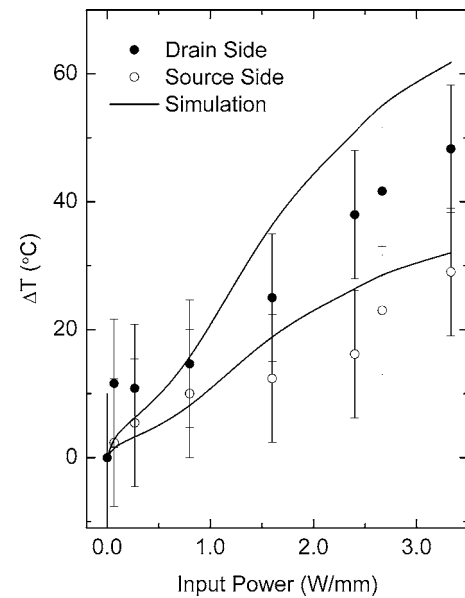


FIG. 8. Measured and simulated rises in temperature on the drain (filled circles) and source (open circles) sides of the gate.

the self-heating of the device. Simulations agree well with the measured dependences in each case examined.

Distinct heating regions partitioned by the vertical dotted lines correspond to the regions denoted on the I - V characteristics in Fig. 1. The low power range of region I corresponds to the Ohmic regime of the device. Approaching the dotted line, the 2DEG becomes depleted at the drain (see Fig. 5). The high field in this power spike volume results in saturation of the electron velocity. For temperature dependent thermal conductivity, $\kappa \sim 1/T$, a quadratic dependence is expected in ΔT versus power across the Ohmic region. Region II is above saturation, and beyond this point, additional power supplied to the device is dissipated within the power spike of Fig. 6(a) creating the hot spot illustrated in Fig. 6(c). In this region we observe slower temperature rise. There are two reasons for this observed slower temperature rise. First, increase in power input causes a shift in the power spike position towards the source side, i.e., under the gate. Second, the $1/T$ dependence of thermal conductivity of GaN results in increase in the high power dissipation in the hot spot resulting in higher temperature particularly in the hot spot. This scenario results in larger gradient in the temperature of the hot spot. Collectively these two factors explain the slower temperature rise observed by the fixed micro-Raman probe which samples a diminishing portion of the hot spot as input power increases.

In order to directly examine the importance of the hot spot in the measured temperature dependence of the device and to test the simulation for lateral heat dissipation properties, we carried out measurements on the drain and source sides of the device.³² The drain-source voltage is varied with the gate bias held at ground. The results from visible micro-Raman measurements are shown in Fig. 8. The curves are results of the coupled electrical and thermal simulations, as described in Sec. IV, with temperature averages taken on the respective sides of the gate electrode. The drain side temperature rise is consistently about twice that of the source

side across the entire input power range. Our results are consistent with recent reports mapping the temperature across the source-gate and gate-drain windows under fixed drive conditions.¹⁴ This temperature difference directly confirms the presence of the hot spot at the edge of the gate on the drain side and its importance in the self-heating properties. In addition, the results further establish the validity of the thermal simulation for describing the dissipation downward through the GaN and substrate and laterally through the device structure.

VI. SUMMARY

We have described a method for micro-Raman measurements using both below and above band gap excitations for studying the self-heating in an AlGaIn/GaN HFET device structure. This approach allows us to evaluate the temperature rise in the 2DEG regime of the device, in the bulk of the GaN layer, and in the SiC substrate. A variety of AlGaIn/GaN HFET drive conditions (V_{DS} and V_g) are examined. Model studies simulating the electrical and thermal behavior have been developed incorporating the 2DEG current confinement, electron velocity saturation, and thermal effect. We obtain excellent agreement with measured temperatures. We note that the maximum ΔT values measured using UV light are very high in comparison to our own visible Raman measurements¹³ and those previously reported.^{12,33,34} Furthermore, the simulations project that the *immediate* hot spot region exhibits a much higher temperature than values obtained in the UV Raman studies. For example, under the highest drive power in Fig. 7, the simulated hot spot $\Delta T \approx 240$ °C while the UV and visible measurements give 130 and 55 °C, respectively, thus illustrating the importance of local heating.

The large temperature rises we conclude are in contrast to previous simulations which suggested relatively small vertical temperature gradients.³³ However, these prior studies relied on lateral mapping by *visible* Raman, combined with thermal FE simulations (only) and assumed constant power density along the width of the gate localized to 1 μm long strip at the edge of the gate. Our electrical simulations show that the Joule heat power density is confined to a much smaller (~ 0.1 μm) strip, which is consistent with Ref. 35. We conclude that temperature depth profiling provides critical information for understanding self-heating in these high power devices. Coupled electrical and thermal simulations describe accurately the power and heat distributions in the HFET. Combined, the temperature depth profiling and the simulations provide detailed understanding of heat dissipation in the AlGaIn/GaN HFET device.

ACKNOWLEDGMENTS

The authors wish to thank S. R. Kurtz for providing the device structures and for numerous helpful discussions. The authors also thank H. Morkoç for thoroughly reading the manuscript. Support from the National Science Foundation

(ECS-0323640) is gratefully acknowledged. One of the authors (I.A.) acknowledges current support from the AFOSR.

- ¹H. Morkoc, *Nitride Semiconductors and Devices*, 2nd ed. (Springer, Berlin, 2006).
- ²S. R. Kurtz, A. A. Allerman, D. Koleske, A. G. Baca, and R. D. Briggs, *J. Appl. Phys.* **95**, 1888 (2003).
- ³M. A. Khan, A. Bhattarai, J. N. Kuznia, and T. D. Olson, *Appl. Phys. Lett.* **63**, 1214 (1993).
- ⁴M. A. Khan, X. Hu, A. Tarakji, G. Simin, J. Yang, R. Gaska, and M. Shur, *Appl. Phys. Lett.* **77**, 1339 (2000).
- ⁵M. E. Levinshtein, S. L. Romyantsev, and M. Shur, *Properties of Advanced Semiconductor Materials* (Wiley, New York, 2001).
- ⁶J. Zou, D. Kotchetkov, A. A. Balandin, D. I. Florescu, and F. H. Pollak, *J. Appl. Phys.* **92**, 2534 (2002).
- ⁷F. Sacconi, A. Di Carlo, P. Lugli, and H. Morkoc, *IEEE Trans. Electron Devices* **48**, 450 (2001).
- ⁸U. V. Bhapkar and M. S. Shur, *J. Appl. Phys.* **82**, 1649 (1997).
- ⁹A. J. Kent and J. K. Wigmore, in *Electron-Phonon Interactions in Low-Dimensional Structures*, edited by L. Challis (Oxford University Press, Oxford, 2003), Chap. 2.
- ¹⁰Y. F. Wu *et al.*, *IEEE Electron Device Lett.* **25**, 117 (2004).
- ¹¹J. Park, M. W. Shin, and C. C. Lee, *IEEE Trans. Electron Devices* **51**, 1753 (2004).
- ¹²Y. Ohno, M. Akita, S. Kishimoto, K. Maezawa, and T. Mizutani, *Jpn. J. Appl. Phys., Part 2* **41**, L452 (2002).
- ¹³I. Ahmad, V. Kasisomayajula, M. Holtz, J. M. Berg, S. R. Kurtz, C. P. Tigges, A. A. Allerman, and A. G. Baca, *Appl. Phys. Lett.* **86**, 173503 (2005).
- ¹⁴J. W. Pomeroy, M. Kuball, M. J. Uren, K. P. Hilton, R. S. Balmer, and T. Martin, *Appl. Phys. Lett.* **88**, 023507 (2006).
- ¹⁵M. Holtz, J. C. Carty, and W. M. Duncan, *Appl. Phys. Lett.* **74**, 2008 (1999).
- ¹⁶J. Wagner, H. Obloh, M. Kunzer, M. Maier, K. Köhler, and B. Johs, *J. Appl. Phys.* **89**, 2779 (2001).
- ¹⁷A. Link *et al.*, *J. Appl. Phys.* **86**, 6256 (1999).
- ¹⁸R. R. Reeber and K. Wang, *J. Mater. Res.* **15**, 40 (2000).
- ¹⁹H. Tang and I. P. Herman, *Phys. Rev. B* **43**, 2299 (1991).
- ²⁰D. Y. Song, M. Basavaraj, S. Nikishin, M. Holtz, V. Soukhoveev, A. Usikov, and V. Dmitriev, *J. Appl. Phys.* (in press).
- ²¹A. Taylor and R. M. Jones, in *Silicon Carbide—A High Temperature Semiconductor*, edited by J. R. O'Connor and J. Smilens (Pergamon, London, 1960).
- ²²J. Liu and Y. K. Vohra, *Phys. Rev. Lett.* **77**, 1661 (1996).
- ²³APSYS, version 2003. 12. 2003, Crosslight Inc., 2003.
- ²⁴E. M. Azoff, *IEEE Trans. Electron Devices* **36**, 609 (1989).
- ²⁵W. R. Frensley and H. Kroemer, *Phys. Rev. B* **16**, 2642 (1977).
- ²⁶M. Farahmand *et al.*, *IEEE Trans. Electron Devices* **48**, 535 (2001).
- ²⁷S. Rajasingam, J. W. Pomeroy, M. Kuball, M. J. Uren, T. Martin, D. C. Herbert, K. P. Hilton, and R. S. Balmer, *IEEE Electron Device Lett.* **25**, 456 (2004).
- ²⁸ANSYS Inc., Release 8.0., 2003.
- ²⁹N. Faleev, I. Ahmad, M. Holtz, H. Temkin, and Y. Melnik, *J. Appl. Phys.* **98**, 123508 (2005).
- ³⁰E. K. Sichel and J. I. Pankove, *J. Phys. Chem. Solids* **38**, 330 (1977).
- ³¹K. A. Filippov and A. A. Balandin, *MRS Internet J. Nitride Semicond. Res.* **8**, 1 (2003).
- ³²Measurements accomplished by reversing the roles of the drain and source to maintain precise positioning of the micro-Raman probe. Ample time was allowed for the device temperature to equilibrate.
- ³³M. Kuball, J. M. Hayes, M. J. Uren, T. Martin, J. C. H. Birbeck, R. S. Balmer, and B. T. Hughes, *IEEE Electron Device Lett.* **23**, 7 (2002).
- ³⁴M. Kuball, S. Rajasingam, A. Sarua, M. J. Uren, T. Martin, B. T. Hughes, K. P. Hilton, and R. S. Balmer, *Appl. Phys. Lett.* **82**, 124 (2003).
- ³⁵N. Braga, R. Mickevicius, R. Gaska, X. Hu, M. Shur, M. A. Khan, G. Simin, and J. Yang, *J. Appl. Phys.* **95**, 6409 (2004).